Article ID: 1000-324X(2021)03-0325-07 **DOI:** 10.15541/jim20200116

Facilely Anchoring Cu nanoparticles on WO_3 Nanocubes for Enhanced Photocatalysis through Efficient Interface Charge Transfer

XIONG Jinyan[1], LUO Qiang[2], ZHAO Kai[3], ZHANG Mengmeng[2], HAN Chao[4], CHENG Gang[2]

(1. College of Chemistry and Chemical Engineering, Wuhan Textile University, Wuhan 430073, China; 2. School of Chemistry and Environmental Engineering, Wuhan Institute of Technology, Wuhan 430073, China; 3. School of Materials Science and Hydrogen Energy, Foshan University, Foshan 528000, China; 4. Institute for Superconducting and Electronic Materials, University of Wollongong, NSW 2500, Australia)

Abstract: Non-noble metal decoration is a promising strategy for promoting semiconductor photocatalysis by effectively enhancing charge separation. Cube-like WO_3-Cu hybrid was successfully synthesized by a facile ascorbic acid reduction method at room temperature. The composition and morphology characterization showed that the Cu particle was deposited on the surface of WO_3 nanocube. The WO_3-Cu-1.0 hybrid (when 1.0 mmol $CuSO_4·5H_2O$ was involved into the reaction system) exhibited promoted photocatalytic capability towards Congo Red photodegradation under simulated sun light irradiation. The trapping experiments of active species during photocatalysis and ESR spectra of DMPO•OH signal of WO_3-Cu-1.0 composite confirmed that the photogenerated holes (h^+), •OH, and $•O_2^-$ were the predominant active species during Conge Red degradation. Based on the photo/electro-chemical measurements, it was proposed that efficient charge transfer was accomplished between the WO_3 nanocube and Cu nanoparticles, which promoted electron-holes separation and subsequently photocatalysis reaction in the Congo Red solution. This work provides a facile preparation method for a binary photocatalyst system in which a semiconductor coupled with non-noble metal.

Key words: semiconductors; metallic composites; WO_3-Cu nanocomposites; pollutants degradation; photocatalysis

The emergence of semiconductor-based photocatalysis has drawn increasing interest because of its universal applications in environmental remediation and solar energy utilization[1-2]. As a visible-light responsive photocatalyst, WO_3 has been widely used with the advantages of non-toxic and stable chemical properties, photocorrosion resistance and photosensitivity[3-7]. However, pristine photocatalyst WO_3 always exhibit fast electron-hole recombination for its inherent physicochemical properties under light irradiation. This phenomenon could result in difficulty in the utilization of photo-generated electrons to generate active species and increase the electron-hole recombination rate, which greatly limits its application in the field of photocatalysis.

To solve the problem mentioned above, noble metal loading is one of commonly used approaches to achieve better charge separation for efficient photocatalysis[8-11]. For example, Xi, *et al.*[11] reported the noble-metal particles grown on WO_3 could facilitate the photogenerated electron-hole separation process due to high electron conductivity of the metal particles. However, the high cost and limited abundance of noble metal hinder their wide application, non-noble metals were applied as alternative ones. The introduction of low valence copper has also been proved as a powerful method for improving photocatalytic activity[12-15].

Recently, much attention has been paid to promoting the photocatalytic activity of cube-like WO_3 nanostructure by coupling with noble metal or other semiconductors[16-18]. Inspired by this background and current challenge, non-noble metal Cu decorated WO_3 nanocube was designed in this work at room temperature. The photocatalytic performance of the WO_3-Cu hybrid was evaluated, and the contribution to the photocatalysis enhancement was also discussed.

Received date: 2020-03-06; **Revised date:** 2020-07-14; **Published online:** 2020-08-01
Foundation item: Hubei Provincial Natural Science Foundation (2019CFB386) 湖北省自然科学基金(2019CFB386)
Biography: XIONG Jinyan(1986–), female, PhD. E-mail: xjybear@163.com
熊金艳(1986–), 女, 博士. E-mail: xjybear@163.com
Corresponding author: CHENG Gang, PhD, associate professor. E-mail: gchenglab@163.com
程 刚, 博士, 副教授. E-mail: gchenglab@163.com

1 Experimental section

1.1 Materials synthesis

In synthesis of WO_3 nanocube, 3.0 g $Na_2WO_4{\cdot}2H_2O$ was firstly dissolved in 65 mL H_2O. Then, 15 mL HCl (37%) was added into the solution gradually under vigorous magnetic stirring for 30 min. The resulting suspension was transferred to a 100 mL Teflon-lined autoclave and maintained at 180 ℃ for 10 h. After cooling down to room temperature, the precipitant was centrifuged and washed thoroughly with deionized water and ethanol for several times, and finally was dried at 60 ℃ overnight[17].

In fabrication of WO_3-Cu hybrid, 0.2 g WO_3 was firstly put into a round bottle containing 10 mL deionized water and 10 mL ethylene glycol. After sonication, 0.03 mmol $CuSO_4{\cdot}5H_2O$ was dissolved into the solution under sonication. Then, 10 mL 0.5 mol/L ascorbic acid aqueous solution was gradually dropped into the above solution and further stirred for 2 h. Finally, the solid product was centrifuged and washed thoroughly with deionized water and ethanol for several times, and was dried at 60 ℃ overnight. This sample was denoted as WO_3-Cu-0.03. When 0.08, 0.3, 1.0, 3.0 mmol $CuSO_4{\cdot}5H_2O$ was involved into the reaction system, the sample was denoted as WO_3-Cu-0.08, WO_3-Cu-0.3, WO_3-Cu-1.0, WO_3-Cu-3.0, respectively.

1.2 Characterizations

X-ray powder diffraction (XRD) was carried out on a Bruker D8 Advance diffractometer by using Cu Kα radiation at a scan rate of 10 (°)/min in the 2θ range from 10° to 80°. Scanning electron microscopy (SEM) image was conducted on a JSM 5510LV at the operating voltage of 5 kV. The energy-dispersive X-ray spectrum (EDX) analysis was carried out on an Oxford Instrument INCA with a scanning range from 0 to 20 kV. Transmission electron microscopy (TEM) images were visualized on a JEM-2000, using an accelerating voltage of 200 kV. The Electron Spin Resonance (ESR) was performed on a Hitachi ESR spectrometer (JES, FA200). The transient photocurrent density and electrochemical impedance spectra (EIS) were analyzed on a CHI660E electrochemical workstation with a standard three-electrode system according to previous study[19].

1.3 Photocatalysis test

In a typical photocatalysis test, 0.02 g catalyst was added into a reactor containing CR solution (40 mL, 20 mg/L) and sonicated to get homogeneous solution. Then, it was stirred for 1 h in the dark to reach adsorption-desorption equilibrium. Subsequently, the reactor with WO_3-Cu catalyst and CR solution was exposed to simulated sun light irradiation by a 500 W Xe lamp with magnetically stirring. 3 mL of the suspensions at each irradiation time interval was collected and then centrifuged. The collected upper solution was analyzed by a Shimadzu UV2800 spectrophotometer.

2 Results and discussion

Fig. 1(a) shows the photographs of the as-synthesized WO_3-Cu samples. It can be observed that the color gradually deepens with the increase of Cu content. As shown in Fig. 1(b), all diffraction peaks of the samples can be assigned with the standard pattern of WO_3 (JCPDS 72-677), indicating that the hybrid contained the main phase of WO_3. The symbol of ★ corresponds to the Cu species in the XRD patterns. With Cu amounts increasing, the diffraction peak of Cu occurred and the intensity became stronger. This result suggested that WO_3-Cu hybrid be successfully prepared through the ascorbic acid reduction method at room temperature.

As shown in Fig. 2(a), the UV-Vis diffuse reflectance spectra demonstrate that the WO_3 nanocube have absorption edge in the visible light region. Compared to pure WO_3 product, a red shift to higher wavelength in the absorption edge of WO_3-Cu hybrids was observed. Fig. 2(b) reveals the band gap of the pure WO_3 is about 2.49 eV. With the content of Cu increasing, the obtained WO_3-Cu sample showed a narrow band gap. This result

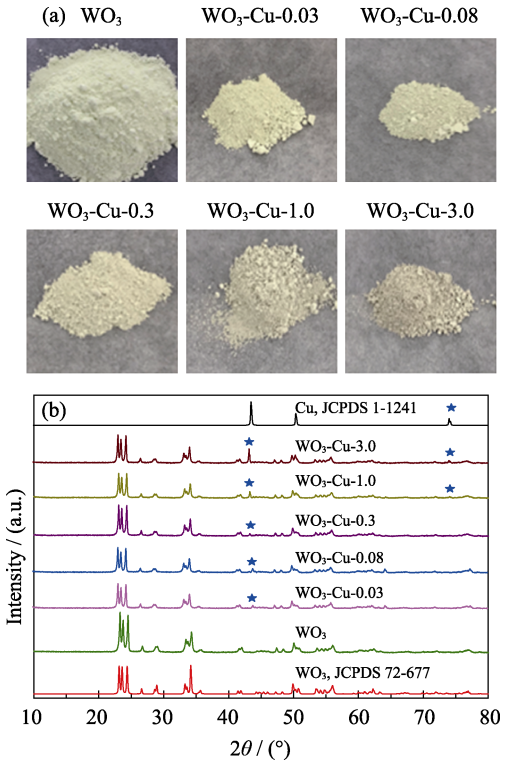

Fig. 1 (a) Photographs and (b) XRD-patterns of WO_3-Cu samples

further confirms that the WO_3-Cu hybrids are successfully synthesized. The valence band (E_{VB}) and conduction band (E_{CB}) edge of WO_3 sample at the point of zero charge can be calculated by the empirical equation $E_{VB}=X-E^e+0.5E_g$, where X is the electronegativity of the semiconductor, E^e is the energy of free electrons on the hydrogen scale (about 4.5 eV), E_g is the band gap energy of the semiconductor, and E_{CB} can be determined by $E_{CB}=E_{VB}-E_g$[20-23]. Based on the above equation and the DRS spectra, the E_{CB} and E_{VB} of WO_3 sample were calculated to be 0.83 and 3.38 eV. Under the visible-light irradiation, because the holes in the VB of WO_3 (3.83 eV) locate at the potential positions lower than those of OH–/•OH couple (2.70 eV)[24], which could oxidize OH^- or H_2O to form •OH and initiate the occur of the photocatalysis reaction.

As depicted in Fig. 3(a, b), the WO_3-Cu-1.0 hybrid exhibited the same morphology with pure WO_3. The

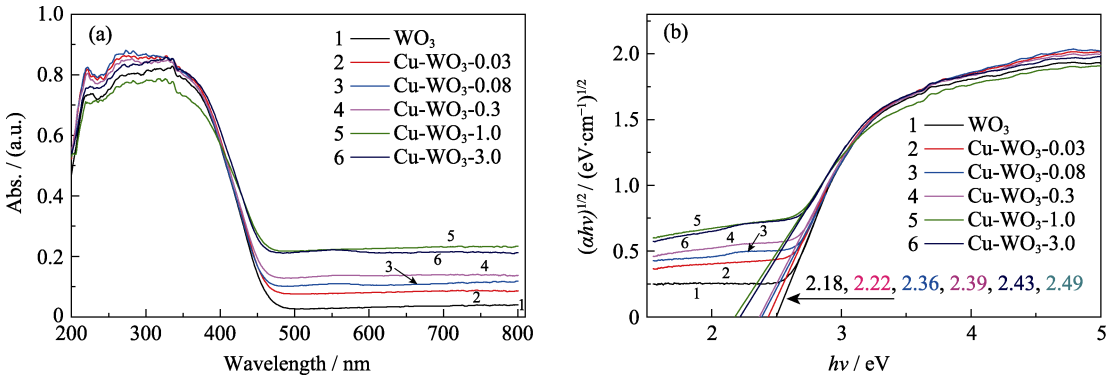

Fig. 2　(a) UV-Vis diffuse reflectance spectra (DRS) and (b) plots of $(ahv)^{1/2}$ *vs* the photon energy (hv) for the WO_3-Cu hybrid and WO_3 nanocube

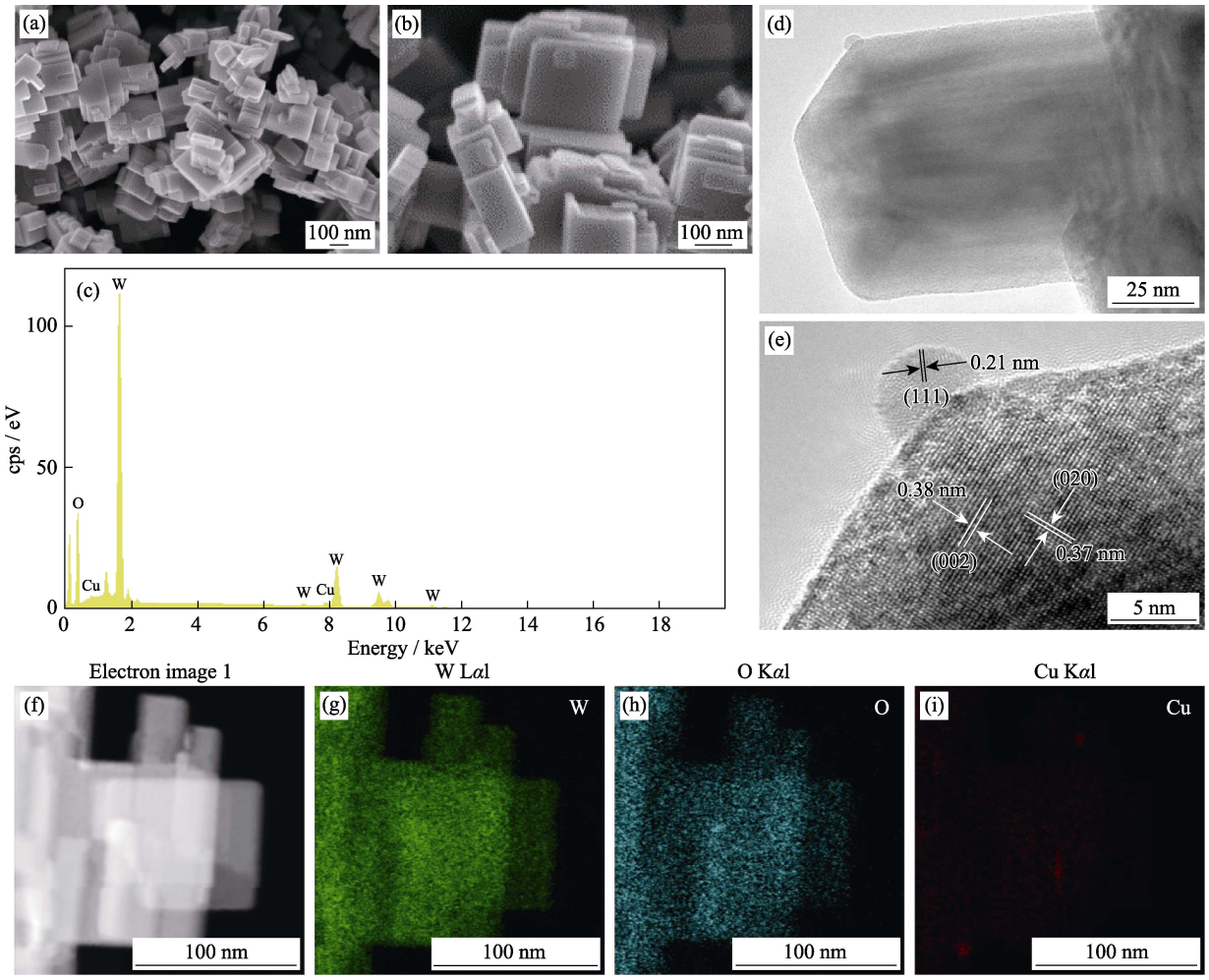

Fig. 3　SEM images of (a) WO_3 and (b) WO_3-Cu-1.0 sample, (c) EDX spectrum of WO_3-Cu-1.0 sample, (d) TEM and (e) HRTEM images of WO_3-Cu-1.0 sample, and (f-i) EDX mappings of WO_3-Cu-1.0 sample

EDX-spectrum (Fig. 3(c)) was also performed to analyze the compositions of the WO_3-Cu-1.0 hybrid. It illustrates that the sample is composed of W, O and Cu, which is in good agreement with the XRD result. The structure of the WO_3-Cu-1.0 hybrid was further confirmed by TEM images. As revealed in Fig. 3(d, e), the Cu particle was deposited on the surface of WO_3 nanocube in the hybrid. Fig. 3(e) displays the HRTEM image of an individual WO_3 nanocube decorated with Cu particle. The clear lattice fringes of 0.37 and 0.38 nm, which correspond to the (020) and (002) crystal planes of WO_3, respectively. On the surface of WO_3 nanocube, the lattice *d*-spacing of 0.21 nm assigned well with the (111) crystal plane of Cu. In addition, as shown in Fig. 3(g, i), Cu, O, W elements were found in terms of the selected area. This result also indicated that the hybrids of Cu particles deposited on WO_3 nanocubes were successfully obtained.

Fig. 4(a) shows the variation in Congo Red (CR) concentration (C/C_0) *versus* irradiation time upon different samples under simulated sun light irradiation. It was found that the WO_3-Cu hybrid displayed superior photocatalytic performance than pure WO_3, while the Congo Red cannot be removed by direct photolysis process. Furthermore, the WO_3-Cu-1.0 exhibited the best performance among the hybrids, and it could remove 85% Congo Red from the solution. Fig. 4(b) shows a pseudo-first-order model, $\ln(C_0/C_t)=kt$ (where k is the pseudo-first-order constant, t is the reaction time). To understand the reaction kinetics of the CR photodegradation, the k value was listed in Fig. 4(c). It was observed that the WO_3-Cu-1.0 had the highest k, indicating its good photocatalytic activity. In addition, Fig. 4(d) indicates that the WO_3-Cu-1.0 also owns good cycling photodegradation performance.

Fig. 5(a) shows the influence of the addition of the scavengers, including methanol, isopropanol, CCl_4, and N_2, for h^+, •OH, electron, and $•O_2^-$ removal, respectively, on the related photocatalytic property. It was found that the CR photodegradation decreased with involving of methanol, isopropanol, or N_2, while the introduction of CCl_4 had no impact on the photocatalysis. It was proposed that the generated h^+, •OH and $•O_2^-$ were the predominant active species during the photocatalysis process. To exclude dye sensitization process, the colorless organic pollutants such as ciprofloxacin (CIP) antibiotic was selected for evaluating the photocatalytic activity of the WO_3-Cu-1.0 hybrid. As shown in Fig. 5(b), it is hard to remove the ciprofloxacin antibiotic through direct photolysis or in the presence of pure WO_3 product. However, when the WO_3-Cu-1.0 was used as the photocatalyst, about 75% of the ciprofloxacin was removed in 4.5 h. As a matter of fact, the Congo Red cannot be degraded under the light irradiation for 4 h. This result indicated that photocatalysis occurred during the Congo Red removal process. Fig. 5(c) shows the ESR spectra of DMPO•OH signal of WO_3-Cu-1.0 composite. It can be

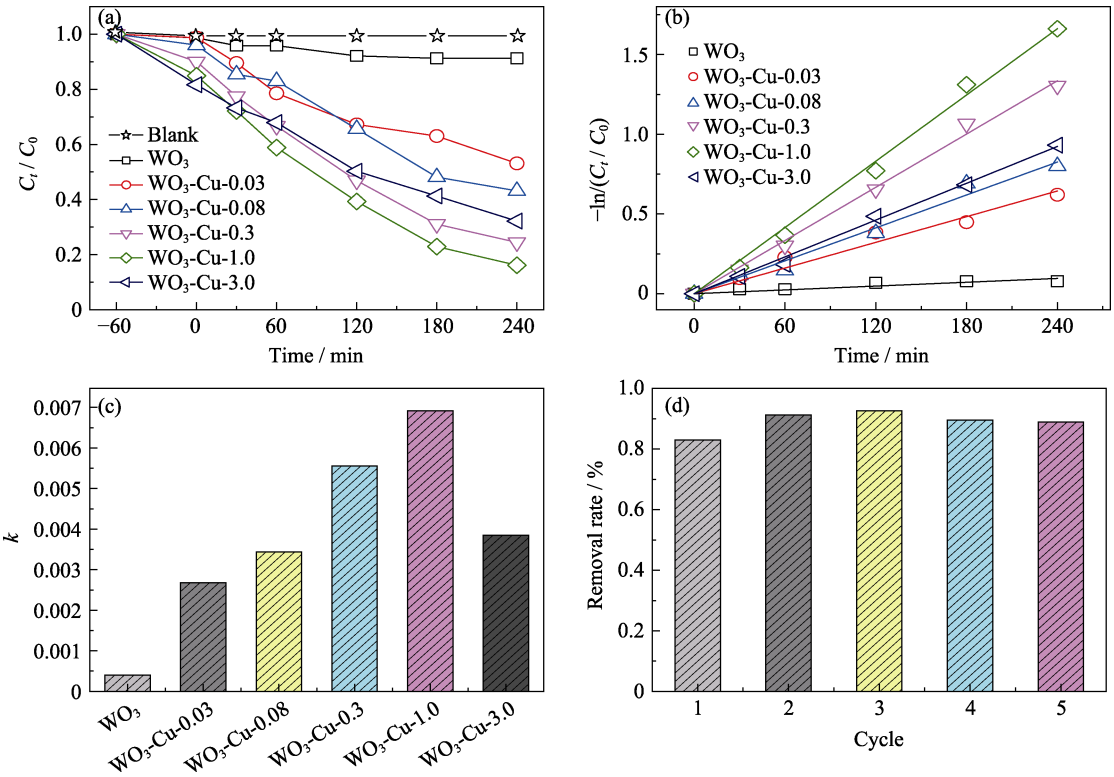

Fig. 4 (a) Photocatalytic performance and (b) CR degradation reaction dynamics of different samples, (c) pseudo-first-order constant k for the different products, and (d) cycling photodegradation of CR upon WO_3-Cu-1.0

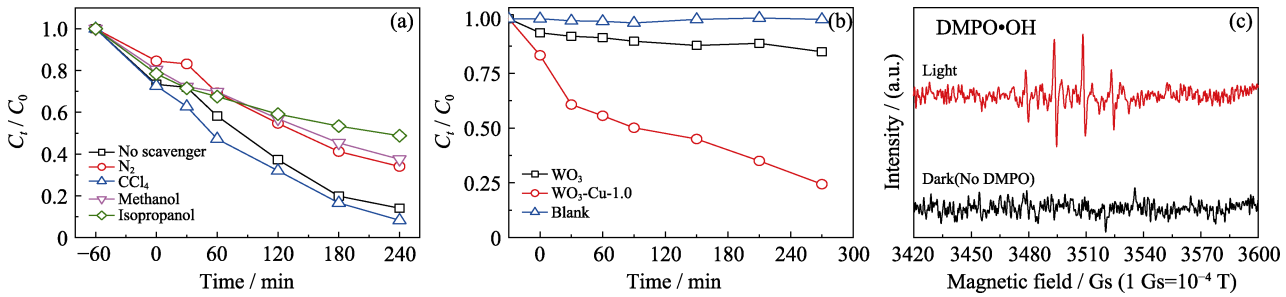

Fig. 5　(a) Effect of scavengers on the photocatalytic degradation and (b) photocatalytic degradation of CIP (40 mL, 20 mg/L) upon WO_3-Cu-1.0 composite (20 mg); (c) DMPO •OH EPR spin-trapping spectra of WO_3-Cu-1.0 composite upon sun light irradiation by a 500 W Xe lamp

clearly observed the obvious characteristic peak of •OH for the WO_3-Cu-1.0 composite upon light irradiation, which further confirms the reactive oxygen species during the Congo Red photodegradation.

The separation efficiency of the electron-hole pairs on pure WO_3 and WO_3-Cu-1.0 hybrid was further studied by photocurrent and EIS experiments. As shown in Fig. 6(a, b), compared to WO_3 nanocube, the WO_3-Cu-1.0 hybrid had smaller arc radius and superior photocurrent. It reflected that the WO_3-Cu-1.0 hybrid exhibited rapid interfacial charge transfer and electron-hole separation efficiency, which contributed to its higher photocatalytic capability[25-29]. On the basis of band gap structure of WO_3 and the scavengers trapping experiment result, a possible pathway for the photocatalytic degradation of CR with WO_3 photocatalyst was proposed as follows:

$$WO_3+h\nu \rightarrow WO_3(e^-_{CB}+h^+_{VB}) \quad (1)$$

$$O_2+WO_3(h^+_{VB}) \rightarrow \bullet OH \quad (2)$$

$$O_2+WO_3(e^-_{CB}) \rightarrow \bullet O_2^- \quad (3)$$

$$Dye_{(ads)}+(\bullet OH,\ \bullet O_2^-,\ \text{and/or}+\ h^+_{VB}) \rightarrow \text{Degradation products} \quad (4)$$

As shown in Fig. 6(c), under visible light illumination, the WO_3 was excited directly, and electrons (e^-_{CB}) and holes (h^+_{VB}) were produced upon the WO_3. Subsequently, e^-_{CB} reacted with the O_2 molecules on the surface to yield reactive oxygen radicals ($\bullet O_2^-$), while h^+_{VB} was directly oxidized to generate •OH. Finally, the CR dye was degraded by the reactive oxygen radicals and/or h^+_{VB}[30-32]. By anchoring Cu nanoparticles on the surface WO_3 of nanocube, the electrons moved to the Cu rapidly and improved the interfacial charge transfer. In other words, the photoinduced electron-hole pairs was separated effectively, and it would produce more reactive species to participate in

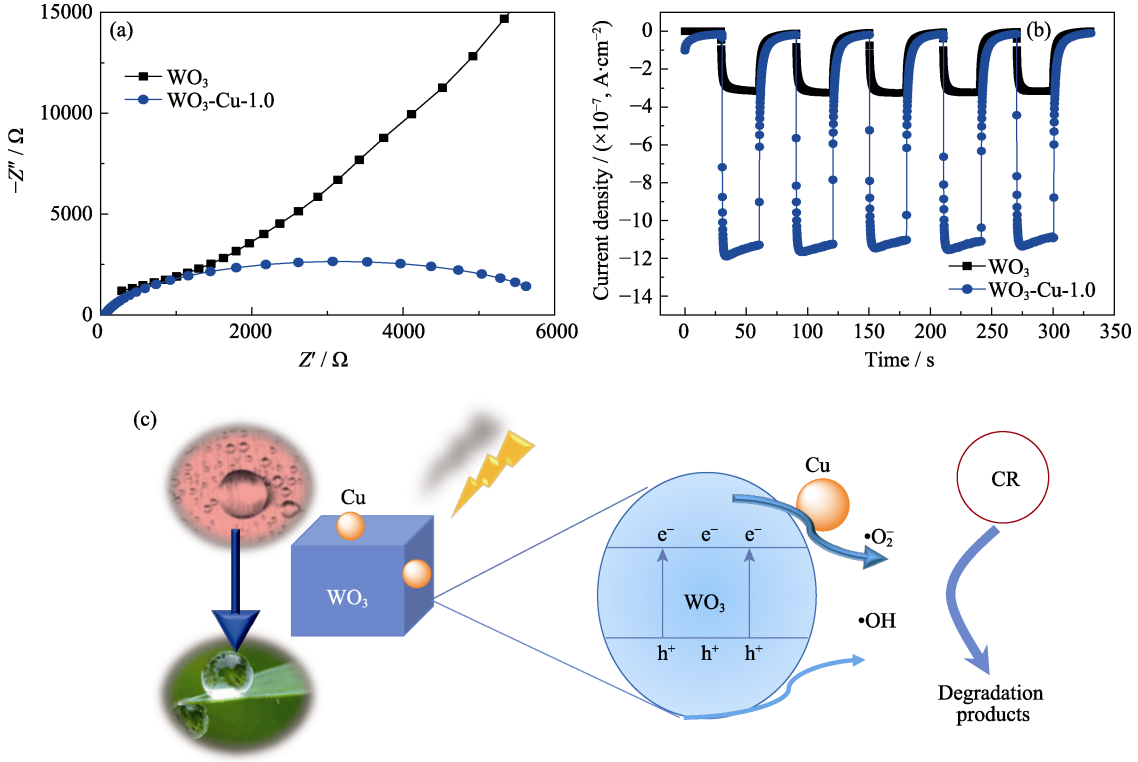

Fig. 6　(a) Photocurrent response and (b) EIS of WO_3 and WO_3-Cu-1.0, and (c) proposed pathways for photocatalytic degradation of Congo Red

the photodegradation process and thus promote efficiency for CR degradation over the WO_3-Cu-1.0 product.

3 Conclusions

In summary, cube-like WO_3-Cu hybrid was successfully fabricated by a facile room temperature method. The involving of Cu particle did not tailor the structure of WO_3 nanocubes, but had impact on its photocatalytic activity. Among the WO_3-Cu hybrid, WO_3-Cu-1.0 showed the highest efficiency towards Congo Red photodegradation. During the photocatalysis process, the generated holes and the •OH were the main active species. Based on photocurrent and EIS measurement, it was concluded that the enhancement of photocatalytic capability was mainly attributable to the higher charge transfer and lower electron-hole recombination of the WO_3-Cu hybrid.

References:

[1] GUO Q, ZHOU C, MA Z, *et al*. Fundamentals of TiO_2 photocatalysis: concepts, mechanisms, and challenges. *Advanced Materials*, 2019**:** 1901997.

[2] MENG X, LIU L, OUYANG S, *et al*. Nanometals for solar-to-chemical energy conversion: from semiconductor-based photocatalysis to plasmon-mediated photocatalysis and photo-thermocatalysis. *Advanced Materials*, 2016, **28(32):** 6781–6803.

[3] HUANG Z F, SONG J, PAN L, *et al*. Tungsten oxides for photocatalysis, electrochemistry, and phototherapy. *Advanced Materials*, 2015, **27(36):** 5309–5327.

[4] SUN S, WATANABE M, WU J, *et al*. Ultrathin $WO_3{\cdot}0.33H_2O$ nanotubes for CO_2 photoreduction to acetate with high selectivity. *Journal of the American Chemical Society*, 2018, **140(20):** 6474–6482.

[5] LIN R, WAN J, XIONG Y, *et al*. Quantitative study of charge carrier dynamics in well-defined WO_3 nanowires and nanosheets: insight into the crystal facet effect in photocatalysis. *Journal of the American Chemical Society*, 2018, **140(29):** 9078–9082.

[6] ZHANG L J, LI S, LIU B K, *et al*. Highly efficient CdS/WO_3 photocatalysts: Z-Scheme photocatalytic mechanism for their enhanced photocatalytic H_2 evolution under visible light. *ACS Catalysis*, 2014, **4(10):** 3724–3729.

[7] ZENG W, CAI T, LIU Y, *et al*. An artificial organic-inorganic Z-scheme photocatalyst WO_3@Cu@PDI supramolecular with excellent visible light absorption and photocatalytic activity. *Chemical Engineering Journal*, 2020, **381:** 122691.

[8] LI Y, LIU Z, GUO Z, *et al*. Efficient WO_3 photoanode modified by Pt layer and plasmonic Ag for enhanced charge separation and transfer to promote photoelectrochemical performances. *ACS Sustainable Chemistry & Engineering*, 2019, **7(14):** 12582–12590.

[9] SUN K, LU Q, MA C, *et al*. Pt modified ultrafine WO_3 nanofibers: a combined first-principles and experimental study. *Materials Letters*, 2019, **236:** 267–270.

[10] GONG H, ZHANG Y, CAO Y, *et al*. Pt@Cu_2O/WO_3 composite photocatalyst for enhanced photocatalytic water oxidation performance. *Applied Catalysis B: Environmental*, 2018, **237:** 309–317.

[11] XI G, YE J, MA Q, *et al*. *In situ* growth of metal particles on 3D urchin-like WO_3 nanostructures. *Journal of the American Chemical Society*, 2012, **134(15):** 6508–6511.

[12] GAWANDE M B, GOSWAMI A, FELPIN F X, *et al*. Cu and Cu-based nanoparticles: synthesis and applications in catalysis. *Chemical Reviews*, 2016, **116(6):** 3722–3811.

[13] ZHU J, ZHANG M, XIONG J, *et al*. Electrostatically assembled construction of ternary TiO_2-Cu@C hybrid with enhanced solar-to-hydrogen evolution employing amorphous carbon dots as electronic mediator. *Chemical Engineering Journal*, 2019, **375:** 121902.

[14] ZHU J, CHENG G, XIONG J, *et al*. Recent advances in Cu-based cocatalysts toward solar-to-hydrogen evolution: categories and roles. *Solar RRL*, 2019, **3:** 1900256.

[15] MALDONADO MI, LÓPEZ-MARTÍN A, COLÓN G, *et al*. Solar pilot plant scale hydrogen generation by irradiation of Cu/TiO_2 composites in presence of sacrificial electron donors. *Applied Catalysis B: Environmental*, 2018, **229:** 15–23.

[16] WANG H, WANG Y, XU A, *et al*. Facile synthesis of a novel WO_3/Ag_2MoO_4 particles-on-plate staggered type II heterojunction with improved visible-light photocatalytic activity in removing environmental pollutants. *RSC Advances*, 2019, **9(60):** 34804–34813.

[17] ZHU W, LIU J, YU S, *et al*. Ag loaded WO_3 nanoplates for efficient photocatalytic degradation of sulfanilamide and their bactericidal effect under visible light irradiation. *Journal of Hazardous Materials*, 2016, **318:** 407–416.

[18] LARA MA, JARAMILLO-PÁEZ C, NAVÍO JA, *et al*. Coupling of WO_3 with anatase TiO_2 sample with high {001} facet exposition: effect on the photocatalytic properties. *Catalysis Today*, 2019, **328:** 142–148.

[19] WEI Y, CHENG G, XIONG J, *et al*. Synergistic impact of cocatalysts and hole scavenger for promoted photocatalytic H_2 evolution in mesoporous TiO_2-NiS_x hybrid. *Journal of Energy Chemistry*, 2019, **32:** 45–56.

[20] MAJHI D, DAS K, MISHRA A, *et al*. One pot synthesis of CdS/BiOBr/$Bi_2O_2CO_3$: a novel ternary double Z-scheme heterostructure photocatalyst for efficient degradation of atrazine. *Applied Catalysis B: Environmental*, 2020, **260:** 118222.

[21] CHENG G, WEI Y, XIONG J, *et al*. Same titanium glycolate precursor but different products: successful synthesis of twinned anatase TiO_2 nanocrystals with excellent solar photocatalytic hydrogen evolution capability. *Inorganic Chemistry Frontiers*, 2017, **4(8):** 1319–1329.

[22] HU C, ZHANG X, LI X, *et al*. Au photosensitized TiO_2 ultrathin nanosheets with {001} exposed facets. *Chemistry – A European Journal*, 2014, **20(42):** 13557–13560.

[23] TIAN J, HAO P, WEI N, *et al*. 3D Bi_2MoO_6 nanosheet/TiO_2 nanobelt heterostructure: enhanced photocatalytic activities and photoelectochemistry performance. *ACS Catalysis*, 2015, **5(8):** 4530–4536.

[24] CHEN Y, HUANG W, HE D, *et al*. Construction of heterostructured g-C_3N_4/Ag/TiO_2 microspheres with enhanced photocatalysis performance under visible-light irradiation. *ACS Applied Materials & Interfaces*, 2014, **6(16):** 14405–14414.

[25] HU X, ZHAO H, LIANG Y, *et al*. Energy level mediation of $(BiO)_2CO_3$ *via* Br doping for efficient molecular oxygen activation and ciprofloxacin photodegradation. *Applied Catalysis B: Environmental*, 2019, **258:** 117966.

[26] WANG X, LI T, YU R, *et al*. Highly efficient TiO_2 single-crystal photocatalyst with spatially separated Ag and F^- bi-cocatalysts: orientation transfer of photogenerated charges and their rapid interfacial reaction. *Journal of Materials Chemistry A*, 2016, **4(22):** 8682–8689.

[27] ZHOU J, LI Y, YU L, *et al*. Facile *in situ* fabrication of Cu_2O@Cu metal-semiconductor heterostructured nanorods for efficient visible-light driven CO_2 reduction. *Chemical Engineering Journal*, 2019,

385: 123940.

[28] WANG M, WANG Q, GUO P, *et al*. *In situ* fabrication of nanoporous $BiVO_4/Bi_2S_3$ nanosheets for enhanced photoelectrochemical water splitting. *Journal of Colloid and Interface Science*, 2019, **534:** 338–342.

[29] WANG Q, ZHANG Y, LI J, *et al*. Construction of electron transport channels in type-I heterostructures of $Bi_2MoO_6/BiVO_4$/g-C_3N_4 for improved charge carriers separation efficiency. *Journal of Colloid and Interface Science*, 2020, **567:** 145–153.

[30] LIU Y, ZHU G, GAO J, *et al*. Enhanced photocatalytic activity of $Bi_4Ti_3O_{12}$ nanosheets by Fe^{3+}-doping and the addition of Au nanoparticles: photodegradation of phenol and bisphenol A. *Applied Catalysis B: Environmental*, 2017, **200:** 72–82.

[31] DIAK M, KLEIN M, KLIMCZUK T, *et al*. Photoactivity of decahedral TiO_2 loaded with bimetallic nanoparticles: degradation pathway of phenol-1-13C and hydroxyl radical formation. *Applied Catalysis B: Environmental*, 2017, **200:** 56–71.

[32] GIANNAKAS AE, ANTONOPOULOU M, DAIKOPOULOS C, *et al*. Characterization and catalytic performance of B-doped, B-N co-doped and B-N-F tri-doped TiO_2 towards simultaneous Cr(VI) reduction and benzoic acid oxidation. *Applied Catalysis B: Environmental*, 2016, **184:** 44–54.

界面电荷快速转移提升铜修饰氧化钨光催化性能

熊金艳[1], 罗　强[2], 赵　凯[3], 张梦梦[2], 韩　朝[4], 程　刚[2]

(1. 武汉纺织大学 化学与化工学院, 武汉 430073; 2. 武汉工程大学 化学与环境工程学院, 武汉 430073; 3. 佛山科学技术学院 材料科学与氢能学院, 佛山 528000; 4. 伍伦贡大学 超导与电子材料研究所, 新南威尔士 2500, 澳大利亚)

摘　要: 非贵金属修饰可以有效增强单一半导体的光生电荷分离, 进而改善光催化活性。采用一种简单的抗坏血酸室温还原法制备了 WO_3-Cu 复合光催化材料, 并用不同表征手段对其组成和结构进行了表征。结果显示, Cu 颗粒沉积在 WO_3 纳米立方的表面, 在模拟太阳光照射下, 与 WO_3 相比, WO_3-Cu 复合材料具有良好的光催化降解刚果红的能力。活性物种捕捉实验以及顺磁共振结果表明, 光诱导产生的空穴、羟基自由基、超氧自由基阴离子等活性物种在刚果红降解过程中起主要作用。根据光电化学测试结果, WO_3 在光催化过程中产生的电子快速转移向 Cu 颗粒, 可以有效分离光生电子–空穴对并加快光生载流子迁移, 进而有利于光催化反应的发生, 从而使 WO_3 表现出较高的光催化活性。

关　键　词: 半导体; 金属复合材料; WO_3-Cu 纳米复合材料; 污染物降解; 光催化

中图分类号: TB33　　**文献标识码**: A